Piotrowski L., Chmielewski M., Golański G., Wieczorek P., Analysis of the possibility of creep damage detection in T24 heat resistant steel with the help of magnetic nondestestructive testing methods, Engineering Failure Analysis, Vol. 102 (2019), pp. 384-394, DOI: 10.1016/j.engfailanal.2019.04.054

Analysis of the possibility of creep damage detection in T24 heat resistant steel with the help of magnetic nondestestructive testing methods.

L. Piotrowski[a], M. Chmielewski[a], G. Golański[b], P. Wieczorek[b]

[a]Faculty of Applied Physics and Mathematics, Gdansk University of Technology, 80-233 Gdansk, Poland

[b]Czestochowa Technical University, Institute of Material Engineering, 42-200 Czestochowa, Poland.

Corresponding author:

Leszek Piotrowski, Gdansk University of Technology, Faculty of Applied Physics and Mathematics, Narutowicza 11/12, 80-233 Gdańsk, Poland

Tel. +(48 58) 348 6617, Fax: (+48 58) 347-28-21

e-mail address: lespiotr@pg.edu.pl

Keywords: creep, magnetoacoustic mission, Barkhausen effect, magnetic methods

Abstract

The paper presents the result of an analysis of applicability of various electromagnetic methods of nondestructive evaluation for creep damage detection in a novel heat resistant steel - T24 grade. Two sample sets, cut out from membrane wall tubes, were investigated – the as-delivered one and another exploited for 36000 hours in a power plant. There are described results of magnetic hysteresis loops B(H), Barkhausen noise (BN) and magnetoacoustic emission (MAE) signals measurements. Changes of the B(H) loops shape are observed mainly in the "knee" regions. The BN signal is practically unaffected by exploitation. The most strongly changing signal is the MAE signal, yet the change is not very easy to quantify as it concerns signal envelopes shape not overall intensity. The paper describes various possible signal parameters that can be used. The best one seems to be the ratio of the total pulse count for a quarter of magnetisation (demagnetisation) to the one for the magnetisation half-period. The important issue is in that case a proper choice of the threshold level in order to obtain good sensitivity to creep damage level and reasonably low stochastic pulse count scatter.

1. Introduction

The failure of industrial components, such as boiler tubes or thick-walled steam pipelines, due the creep damage poses a serious threat to a safe and prolonged exploitation. Being so it very important to search for a way of nondestructive monitoring of their structural health. Such methods may be based on the measurements of magnetoelastic properties of the investigated materials. It has been observed that magnetic hysteresis loops undergo systematic change during creep process, however such a change is observed most clearly while magnetising the sample with an encircling coil – the geometry non-applicable in most cases during in-field

inspection. Another candidate is the Barkhausen noise (BN) signal which has already been proposes for such purpose [1]. This is a signal generated during an abrupt jump of the domain wall (DW) from one pinning site to the other. Such jump results in a local change of magnetisation, which in accordance with Faraday's law becomes a source of changing electric field and finally electromagnetic pulse which can be detected with the help of coil placed close to the surface. Since the jumps are strictly correlated with the pinning sites (precipitates, dislocation tangles) distribution any change of material microstructure should result in BN signal modification. However the main drawback of this method in industrial applications is the fact that as an electromagnetic signal of a kHz range it is strongly attenuated in conducting material, hence the signal may be detected only from the close to surface region (depending on material properties and the BN signal filtering range detection depth may range from tens up to several hundred micrometres [2]). It makes the BN signal very sensitive to surface preparation conditions.

Finally one can analyse the magnetoacoustic emission (MAE) signal changes. The MAE phenomenon was for the first time investigated in a systematic way by Lord [3] in 1975 and has found many possible applications since then. Lo et al. [4] analysed the influence of pearlitic steels microstructure on the MAE signal. Another groups [5,6] investigated the MAE signal potential for the stress level assessment, also with a view to determine residual stress due to plastic deformation [7]. Su [8] proposed a method based on multi-frequency magnetic field generation in order to assess stress distribution inside the material. On the other hand Park et al [9] suggested application for the irradiation monitoring in RPV steels.

The source of the MAE signal are also DWs jumps yet only non-180° (90° in iron alloys) ones take part in the process. It is due to the fact that MAE pulses are caused by an abrupt, local change of material dimensions due to magnetostriction effect. Since magnetostriction is an even function of magnetisation, the 180° DW jump doesn't change the length of remagnetized area.

The fact that only a subpopulation of domain walls is active in the MAE signal generation makes it sensitive to the magnetic field ranges for which this subpopulation is active. This are the magnetic field intensities for which DWs creation/annihilation takes place which correspond with the “knee” portions of hysteresis loops. It is a rather fortunate fact as it was observed that those “knee” areas are most strongly affected by creep. In addition to that the signal, being an ultrasound acoustic signal is weakly attenuated in steels thus allowing to investigate the whole magnetised volume. The earlier attempts made with older steel grades had given promising results [10], suggesting the MAE signal applicability for creep level assessment. The T24 steel is rather a new one so it may remain in service for a long time still thus it would be very useful to find the method suitable for its creep induced changes monitoring. It is however very difficult to get by the well documented exploited, samples hence our study on the samples after only one exploitation period (an as-delivered one) must be treated as only preliminary assessment.

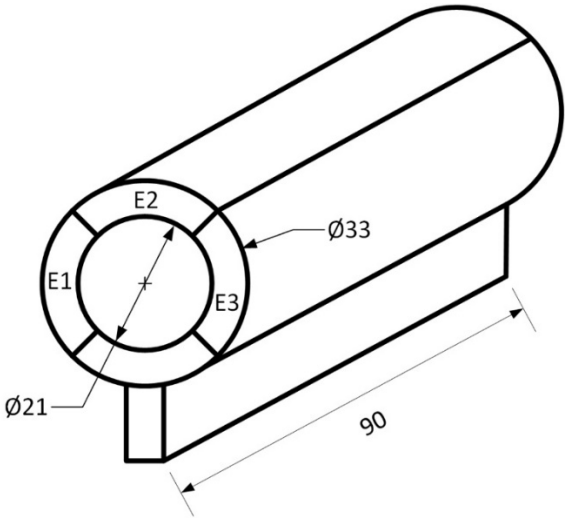

Fig. 1 Cut-out scheme for the exploited samples.

2. **Experimental**

Two sets of three samples each, made of T24 steel (7CrMoVTiB10-10) were investigated. One of them was cut out from the as-delivered pipe, and the other from the fragment of pipe

that had been exploited in a power plant for 36 thousands hours under nominal pressure 23.8 MPa and working temperature 540 °C. The cutting scheme for the latter case is shown in Fig. 1 – the bar, welded to the tube in an assembly process, made a part of it unusable hence only three samples E1-E3 were investigated. In the case of as-delivered sample there was no bar, yet we decided, considering statistical error analysis, to have the same number of samples (three) in both sets choosing randomly three samples N1-N3. The length of the samples was L = 90 mm and wall thickness h = 4mm. Chemical composition of the investigated steel is given in Table 1.

Table 1. Chemical composition of T24 steel [wt.%]

C	Si	Mn	S	P	Cr	Mo	Ni	Ti	V	N
0.07	0.30	0.43	0.004	0.015	2.35	0.97	0.13	0.07	0.22	0.017

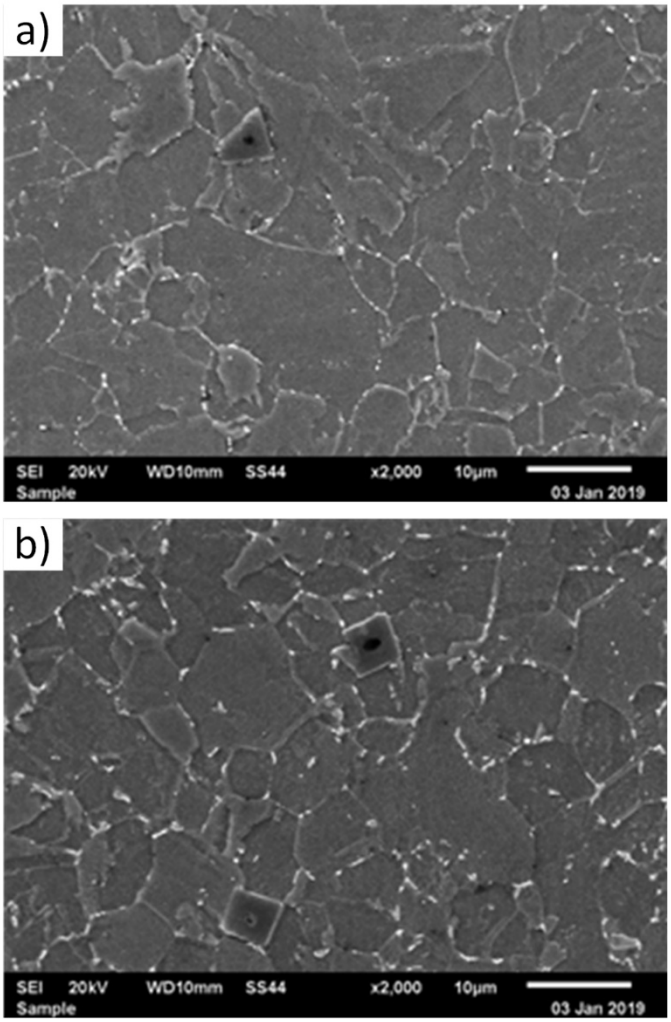

Fig. 2 Microstructure of the T24 steel (SEM): a) as-delivered, b) exploited

The microstructure of the as-delivered sample, shown in Fig. 2a, consisted of granular bainite and ferrite. One can observe characteristic precipitates of titanium nitrides, and in addition to them $M_{23}C_6$ carbides, precipitated at the former austenite and ferrite grain boundaries as well as at bainite laths boundaries. Inside the grains and laths there are small precipitates of the MX type particles. The exploited sample (the degradation level of which can be assessed as an early stage) still consisted of granular bainite and ferrite with TiN precipitates – see Fig. 2b. However, the exploitation process resulted in the increase in number and growth of carbides at grain boundaries. The correlation of the geometrical changes in the structure of precipitates with the literature data [11,12] allows to suppose that inside the grains the precipitation of molybdenum rich M_2C precipitates proceeds. At the same time recovery and

polygonization in the matrix takes place, resulting in the decrease of dislocation density, subgrain structure coarsening and polygonised ferrite appearance.

The Barkhausen noise signal was measured with the help of commercially available MEB 2c apparatus manufactured by Polish company Mag-Lab, described in detail in [13]. The probe of the apparatus consists of a C-core with magnetizing coils (magnetizing frequency f = 25 Hz) and an additional control coil (for the magnetisation quality assessment), wound on it. The magnetizing coil is fed with triangular current. For the detection of the BN voltage signal, a small sensor coil wound on a ferrite core is used. The measured cut out frequency of the detecting coil is about 100 kHz and analog high pass filter frequency (removing the low frequency $d\Psi/dt$ component) is 1 kHz. In order to ensure good contact with the surface the coil is pressed with a spring. However instead of making use of the pre-defined signal parameters (rms and pulse count dependent values) supplied by the apparatus, the noise signal was measured directly with the help of 14 bit PC measurement card (sampling frequency 2MHz).

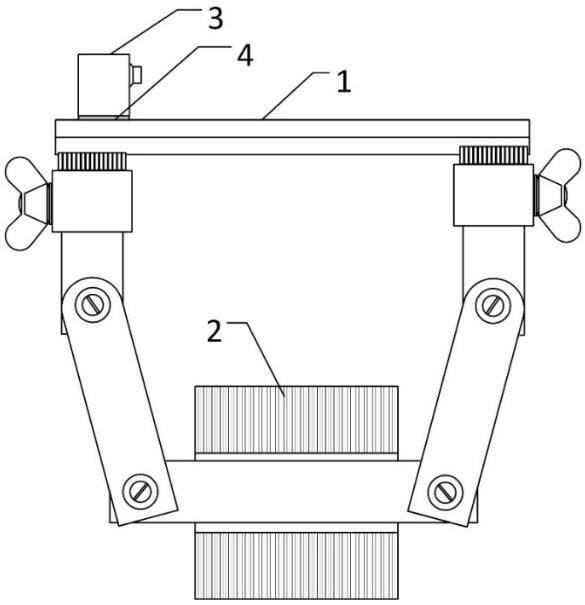

Fig. 3 The experimental set up – MAE measurements

The MAE signal was measured with the help of a set shown in Fig. 3. The sample (1) was magnetised (current triangular in-form, f = 1 Hz) by the electromagnet (2) designed for the

measurements on the curved surfaces (pipes) – described in [14] – the important feature of which are poles made of sets of small sliding rods that can adjust to the local curvature (2D).

For the detection of MAE pulses the wide band (125 -1000 kHz) acoustic emission sensor (3) manufactured by Physical Acoustic Company was placed on the sample surface, the coupling to which was obtained using silicon grease (4). Both the magnetisation (triangular current) and measurement process are controlled by the dedicated apparatus containing NI USB-6353 multifunction device which in turn is driven by the software written in the LabVIEW environment. The device allows for some signal processing, yet in order to analyse the measured signals more thoroughly the amplified noise signal was directly recorded (with sampling frequency 1 MHz). We have made such a choice of devices in order use the measurement configurations that we can most easily apply in the industrial environment.

In addition to that, in order to assess qualitatively the change of magnetic hysteresis loops B(H) of the samples subjected to creep the setup was modified in such a way that the electromagnet was used for the flux closure and the magnetisation was provided by the additional coil surrounding the sample. There was also a smaller coil fitted into the magnetising one that was used for the flux change detection which in turn was used for the Magnetic hysteresis loops shape determination. Such a configuration cannot be naturally used for the absolute B(H) values determination yet it shows clearly the influence of creep damage on magnetic properties.

3. Results

3.1 Magnetic properties

Averaged (over all the samples for each set) magnetic hysteresis loops are shown in Fig. 4. The results are corrected taking into account small differences in sample cross sections. As can be seen, the most pronounced difference between the presented loops is in the ”knee” region of

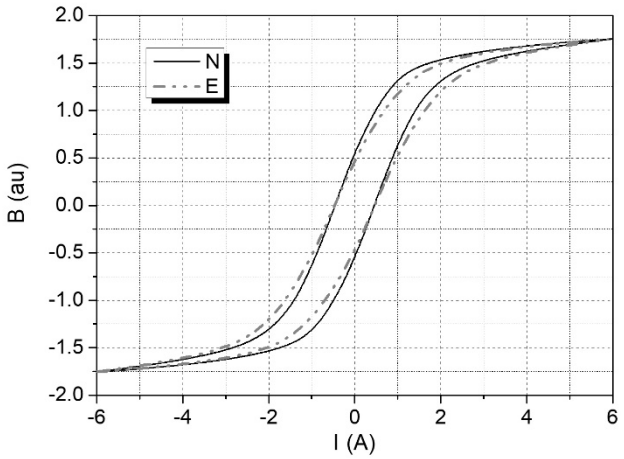

Fig. 4 Averaged hysteresis loops for the tested samples: N – as delivered; E – exploited

the hysteresis loops – this is in a good agreement with the results observed for previously used T22 steel after prolonged exploitation [15]. This is an important feature of the creep damage process, since those regions are expected to be main source of MAE, as one expects the process of creation/annihilation of domain walls to take place at corresponding magnetic field values. Being so, one can expect the differences of MAE signals for both sets of samples to be significant. The results of quantitative analysis of the obtained magnetic hysteresis loops are plotted in (Fig. 5).

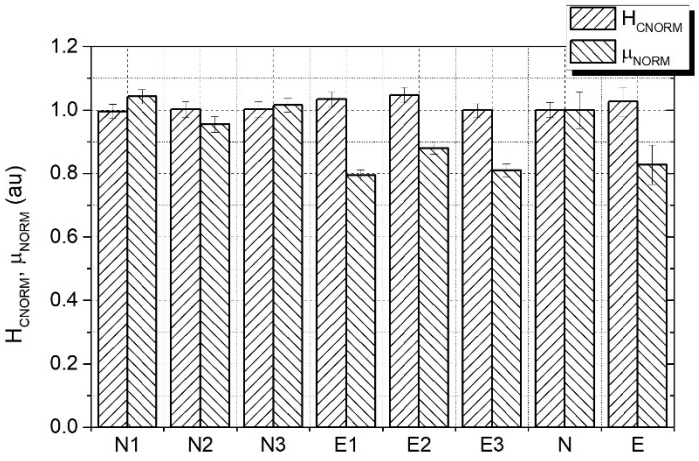

Fig5. Normalized maximum differential permeability and coercivity for the tested samples

Coercivity seems to increase very slightly (by about 2.5% - less than standard deviation) whereas the decrease of permeability is about 18 % (which is definitely more than standard deviation value). Such behaviour is also in agreement with the results presented in [15], provided that the degradation stage of the exploited sample is low. Unfortunately the maximum differential permeability is not easily measured in industrial environment as it is extremely sensitive to the magnetic flux closure quality.

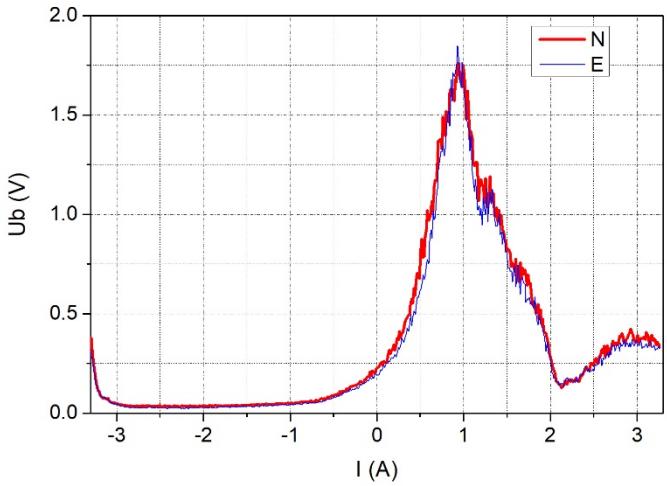

Fig. 6 Averaged BN signal envelopes for the investigated samples (N – as delivered, E - exploited)

3.2 Barkhausen noise signal

The Barkhausen noise signal obtained with the help of MEB 2c apparatus was recorded and then subjected to numerical analysis with the help of a dedicated software working in the LabVIEW environment. We have performed the measurements only on the external side of the samples. We did so for two reasons. Firstly, it is the only accessible surface for the real industrial components. Secondly, due to the cut out method (frame saw) of the samples their sidewalls surface properties may be modified relatively deep. First, the rms-like signal envelopes (rms signal calculated for very short time periods) were determined, unfortunately

the average signals obtained after averaging of 18 envelopes for each sample set (3 measurement series, 3 samples, two measurement areas on the external side of each sample) are almost identical (Fig. 6) – to some degree it may be due to the fact that in the case of measurement sets with small magnetising probe (MEB – 2c, Rollscan[16]) the shape of BN signal envelopes is not strongly affected and the main difference is the signal intensity change. It should be mentioned that the small, sharp maximum for negative filed values is in fact due to the phase shift between the magnetizing current and magnetisation – it would not be present if Ub was plotted vs H field inside the material. Naturally better suited for the signal envelope modification are systems based on encircling magnetizing and pick-up coils, yet such systems are not well suited for industrial applications. The lack of average signal intensity change due to the exploitation process is confirmed by Fig. 7 where the value of parameter:

$$Int(Ub) = \int_{-I_{MAX}}^{I_{MAX}} Ub_0 \, dI; \; where \; Ub_0 = \sqrt{Ub^2 - U_{noise}^2} \qquad (1)$$

is plotted. We treat that signal as a measure of the signal intensity. U_{noise} can be determined finding the minimum value of the envelopes The results for various samples are characterised by high standard deviation (10-20%) and even though there is some difference between them, they are typically of the order of the SD range. The only sample that seems to have noticeably lower BN intensity is sample E3. It might suggest that it is the most creep affected sample.

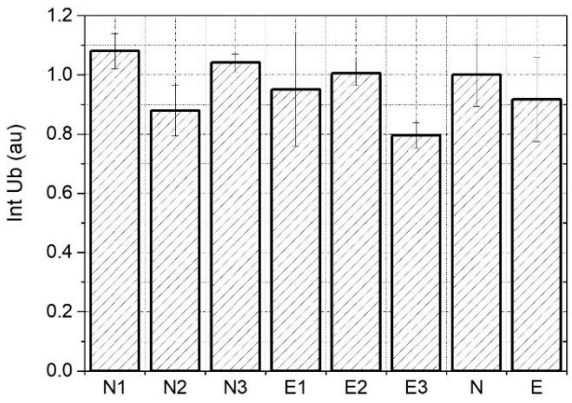

Fig 7. Normalized BN signal intensity for the investigated samples

As the overall intensity analysis had not led to a promising solution we have tried an approach based on pulse count analysis. We have calculated for each period of magnetisation the pulses exceeding threshold value for three threshold levels (0.5; 1.5 and 2.5V). The levels were chosen

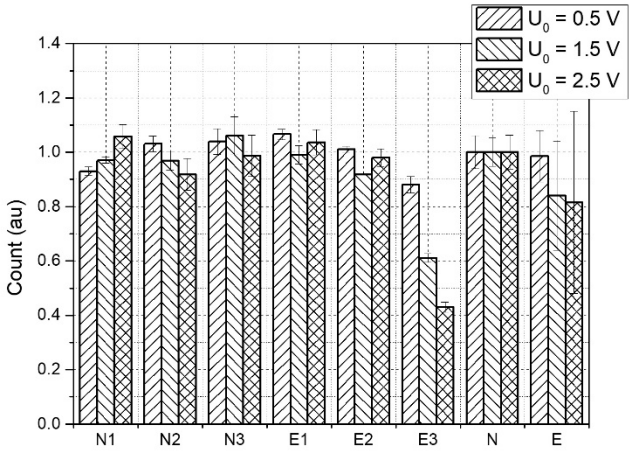

Fig. 8 Normalized BN pulse count number for various threshold levels

in such a way that the lowest one was slightly above the background noise level and the highest one gave reasonably high values of total pulse count – namely of the order of 100-200 counts. The averaged and normalized values of the pulse count value are plotted in Fig. 8. As can be seen the results obtained for low threshold value are similar to the intensity measurement results (in this case we count most of the BN signal pulses) whereas for the higher thresholds values where we take into account only small subset of measured pulses (due to the relatively long DWs jumps) the difference between the E3 sample and the remaining ones is clearly pronounced confirming that this is the sample most different from the rest. The difference is quite high, but one has to bear in mind that BN signal is detected only from the close to surface region of the samples hence it may be affected by the exploitation in a different way than other signals dependent on bulk properties.

3.3 Magnetoacoustic emission signal

The MAE signal is potentially the most suited for the deformation level assessment. It is due to the fact that it can be obtained from the whole magnetised volume and that it is measured with the help of the probe placed on the surface of the investigated tubes/pipes. The only issue is the repeatability of the measurements since the intensity of the measured signal is strongly dependent on the quality of probe – surface contact. In order to verify the influence of this factor the measurement were performed twice (on two different days) so the whole procedure – sample placement, pole shape optimisation and transducer adjustment - had to be repeated. Only this kind of approach can give an estimate of experimental errors in industrial environment since repeating measurements without dismantling the set-up allows only to assess the statistical errors due to stochastic character of MAE signal (and measurement set-up properties), which are much lower than real experimental errors. As it turned out the repeatability was very good as for this kind of measurement procedure.

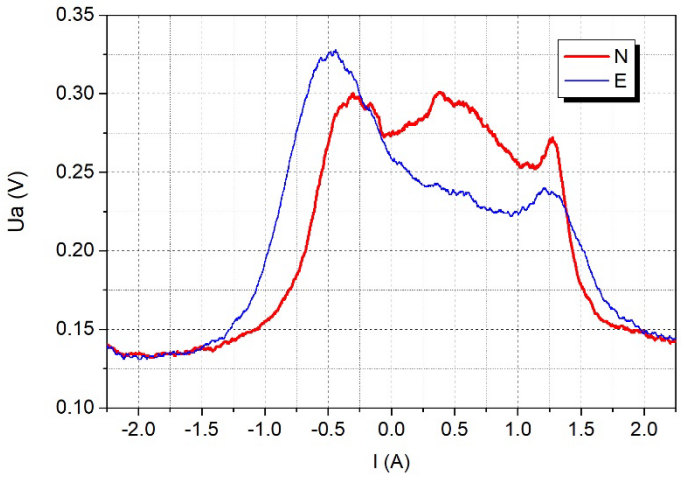

Fig. 9 Averaged MAE signal envelopes for the investigated samples (N – as delivered, E - exploited)

The averaged (3 samples, two measurement series) MAE signal envelopes are plotted in Fig. 9. It can be seen that the shape of the MAE envelopes evolves significantly – initially the signal has three weakly marked maxima of similar height and after exploitation it evolves into

two-peak shape. The first peak is strongly pronounced (it is both high and wide) while the second one is barely visible. The broadening of the signal is an expected consequence of the observed changes of the B(H) hysteresis loops – namely the increased separation of the "knee" portions of the loops. As for the peak structure changes (from 3 to 2) they may be due to the systematic disappearance of two phase structure, yet one has to take into account that for such

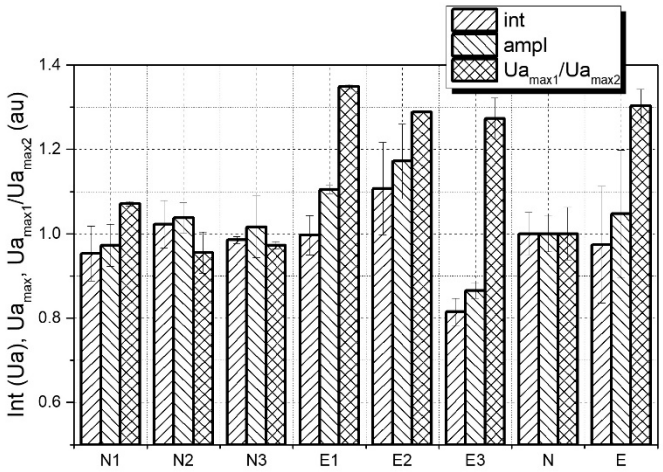

Fig. 10 Normalised parameters of the MAE signal for the investigated samples:

int – intensity, ampl – amplitude, Ua_{max1}/Ua_{max2} – ratio of the first to last maximum

thick samples magnetisation (and as a result the generated MAE signals) phase is strongly shifted in the inner layers of the material hence the observed signal is not truly an intrinsic property of the sample. The exploited sample, having lower permeability, is less affected by the eddy current induced shift. Being so, at least some part of the shape change may be attributed to the macroscopic magnetic properties change. Nonetheless, no matter what the exact nature of envelope shape modification is, it is quite strong and suggest the possibility of creep level deformation assessment with the help of MAE signal measurements.

Unfortunately the observed change cannot be well quantified with the help of the intensity parameter, defined previously (1) for BN signal. The results of such an attempt are shown in Fig. 10, on the average the MAE intensity (int) for the exploited samples is a bit lower, but the

change is much lower than the difference between the intensities for exploited samples. Only the sample E3 can be clearly discerned from the remaining ones (intensity for that sample is significantly lower), and for the E2 sample one observes the increase of the intensity – contrary to the mean value behaviour. It is not surprising since the signal for exploited samples is much stronger than for new ones for negative magnetizing current values (increasing magnetisation) yet the opposite is true for positive current. Being so we tried to analyse the amplitude changes (using Ua_0 signals obtained on the basis of (1) in the same way as in the case of Ub_0), yet the results were similar, the lowest signal was obtained for E3 and the mean value for the exploited samples increased a bit, yet once again less than its standard deviation.

Finally, analysing the obtained envelopes we have decided to determine the changes of purely shape dependent parameter – namely the ratio of the first to the last amplitude. One very important feature of such parameter is that it is weakly dependent on the quality of contact between the MAE probe and the sample surface. An inadequate contact should result in the decrease of both analysed amplitudes more or less proportionally, provided that we analyse the signals after the background level subtraction (Ua_0). This time we finally obtained a parameter that changes very strongly (~30%), with reasonable scatter, thus allowing to unambiguously discern the as-delivered samples from the exploited ones. The only problem with this parameter is the fact that maxima of the signals for as-delivered samples are not always clearly discernible (hence higher standard deviation for the as delivered samples than for the exploited ones). In our case we have used manual detection of the maxima with the help of graphical positioning tool, but one would have to be very careful trying to implement an automatic algorithm in order to identify correctly the maximum.

The next step was the pulse count analysis. Unfortunately it turned out not to give satisfactory results and it cannot be used for the creep assessment (see Fig. 11). Once again the E3 sample was the most different one (the higher the threshold the bigger the relative change),

and the mean value for the exploited samples was observably lower, yet the scatter of the results was very high making that parameter practically useless. The more promising seems to be the analysis of the pulse count rate – the examples of the results obtained for two different threshold levels (0.4 and 0.6V) are shown in Fig. 12. As can be observed the main difference is again in the shape of the plots, what is important the difference becomes more pronounced (relatively)

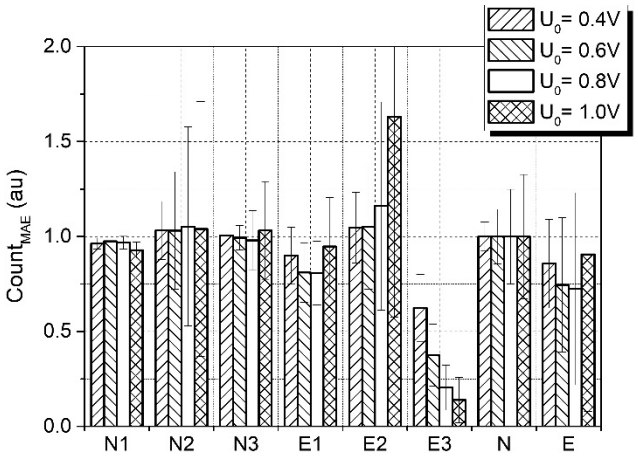

Fig. 11 Total pulse count for the analysed samples (normalized values).

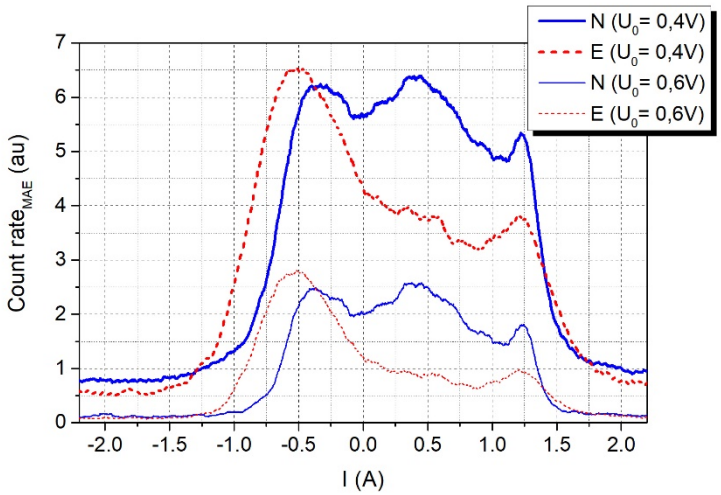

Fig. 12 Pulse count rate for the investigated samples for two different threshold levels.

for the higher threshold levels. This time due to relatively higher scatter of the instantaneous values of pulse count rate than observed for MAE intensity we did not try to measure the

amplitude but proposed the asymmetry parameter based on relative area under the plot calculated for the 1-st (and 3-rd) quarter of magnetisation period, assuming that we start from the fully magnetized state ($-I_{max}$):

$$N_{max-0}/N_{total} = \int_{-I_{max}}^{0} PCR_{MAE}dI / \int_{-I_{max}}^{I_{max}} PCR_{MAE}dI, \quad (2)$$

where PCR stands for the pulse count rate. The as obtained normalised values are plotted in Fig.13. This time the obtained results seem to be quite satisfactory, the observed decrease for the exploited samples is very strong and with reasonable scatter (except for high thresholds for N2 sample). The most reasonable choice seem to be the U = 0.6V threshold level as for this level we have the decrease of the analysed ratio equal to almost 50% with standard deviation of order of 15%.

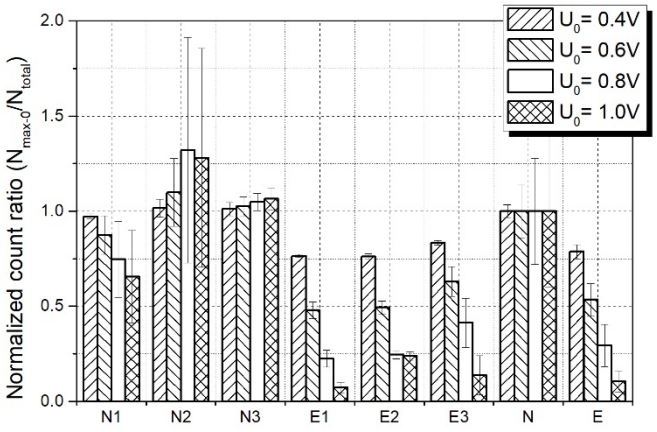

Fig. 13 Normalised count ratio for the investigated samples

We have also tried to verify if the creep degradation process influences the spectrum of the measured signal. In order to do so one can use either the FFT transformation (not best suited for noise signals, yet relatively simple and common approach) or wavelet transformation (taking into account both time and frequency/scale domain). We have decided to choose the wavelet analysis using continuous wavelet transformation. It's results can be easily interpreted

in the domain of coefficients as they reflect the shape of actual signal. The wavelet transformation coefficients are calculated according to the formula [17]:

$$CWT_{coeff}(a,b) = \int_{-\infty}^{\infty} s(t)\psi\left(\frac{t-b}{a}\right)dt, \qquad (3)$$

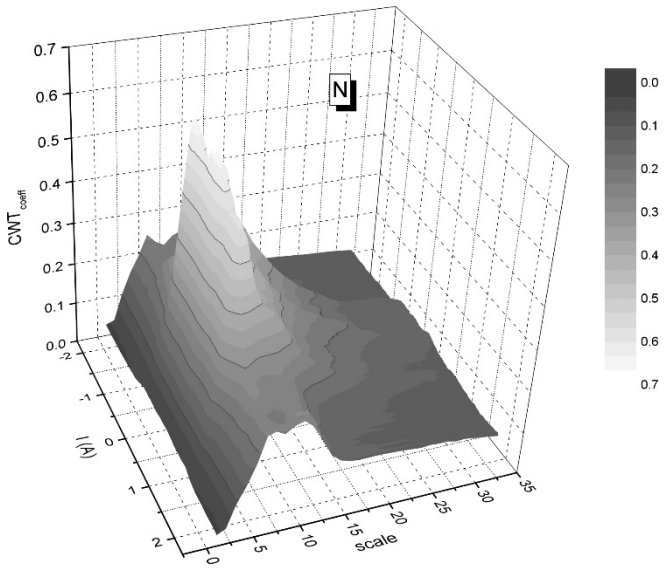

Fig. 14 Averaged CWT (Morlet) coefficients for the as-delivered samples.

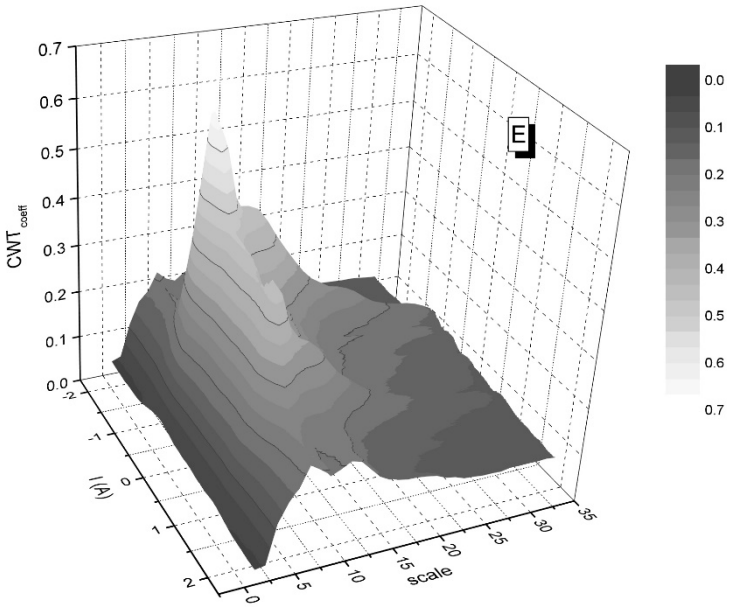

Fig. 15 Averaged CWT coefficients (Morlet) for the exploited samples.

Where *a* determines the scale of the wavelet (the higher the scale the wider the time span of the wavelet). Once the integral is calculated, the wavelet is shifted in time and the procedure is repeated. The *b* parameter determines the translation of the function and gives the time domain localization of a given CWT coefficient. We have chosen Morlet wavelet and performed

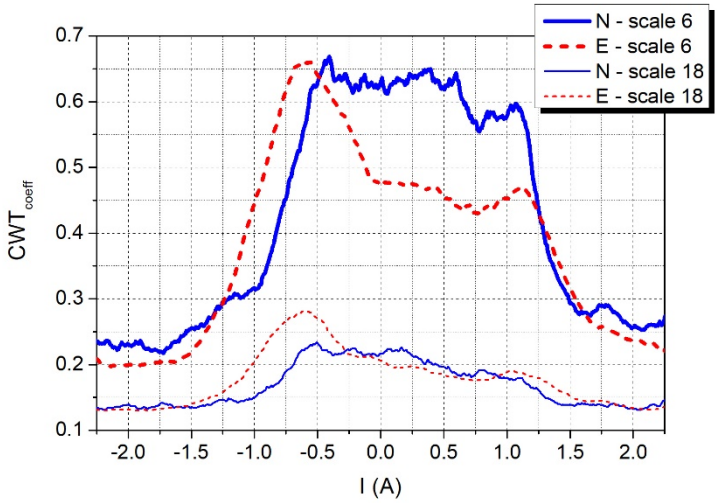

Fig. 16 Averaged CWT coefficients for investigated samples for two different scales

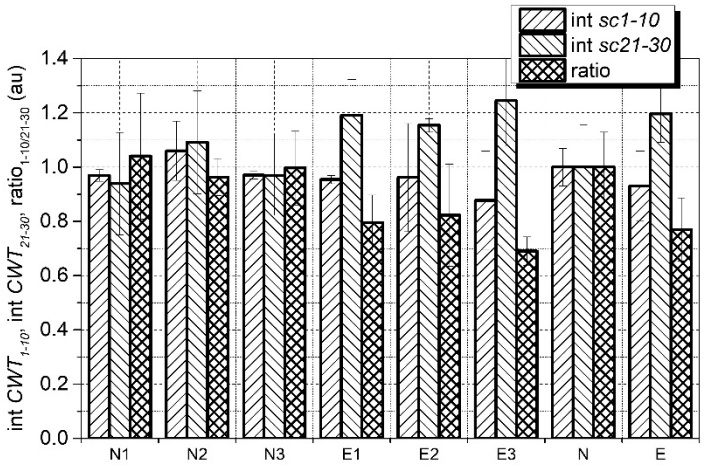

Fig. 17 Average CWT coefficients integrals for various scale ranges and their ratio for the investigated samples

calculations in LabVIEW environment with 50 point time step (25μs) up to 32-nd scale. The averaged CWT coefficients for as-delivered and exploited samples are plotted in Fig. 14 and Fig. 15 respectively. The time scale in both figures was replaced by the magnetizing current intensity I(A) in order to make it comparable with other results. Such replacement was possible because the I(t) dependence is linear. The difference in the time domain for the new and exploited samples is again visible, yet this time we can see that the signal intensity is to some degree scale dependent what can be seen from Fig. 16 in which the CWT coefficients for two different scales are plotted. Being so we have decided to compare the results obtained for various scale ranges (integrating over the time domain averaged CWT coefficients for 1-10 and 21-30 scale ranges respectively) – the results are shown in Fig. 17. Since the obtained integrals behave in a reciprocal way – low scale component slightly decreases and the high scale one increases we have calculated the ratio of low component to the high one and thus obtained a parameter which decreases about 20% and should be, due to its relative nature, independent on the contact quality. It should be mentioned that the results frequency/scale analysis is strongly dependent on the MAE sensor properties. In our case the sensor is not very sensitive to low frequency components. Using the sensor with broader frequency range might lead to better results, especially since the difference for larger scales (lower frequencies) is more pronounced than for the smaller ones.

4. Conclusions

Material properties deterioration due to the creep process is an important problem and possibility of monitoring of its progress in a non-destructive way would be very helpful. The main factor affecting both mechanical and magnetoacoustic properties is the change of precipitate size and distribution. What is important the MAE signal is dependent only on the

interaction of a subpopulation (90°) of DWs with precipitates whereas the BN signal depends on both kinds of walls (yet due to their dominant area it is mainly affected by 180° ones). The 90° DWs for ferritic/bainitic steels are created mainly close to the grain boundaries (closure domains) and the observed increase of precipitate dimensions at the grain boundaries result in the change of DWs dynamics and hence the changes in the MAE signal. On the contrary the BN signal is mostly affected by the changes inside the grains and hence its behaviour may be completely different. At the onset of the creep two processes most strongly affect the BN signal – precipitation of alloy elements from the matrix and coagulation of the precipitates. Their effect on the BN signal intensity is opposite, hence as a result we obtain a completely different behaviour to the one observed for MAE. In our case we have observed that the samples after exploitation have significantly different magnetoelastic properties than the as-delivered ones. One could in principle use classical magnetic properties (measuring B(H) loops) yet it is not easy in an industrial environment. Barkhausen noise signal seems to be useless in that case since it seem to be almost non affected by exploitation for this steel grade. The most promising is the analysis of the magnetoacoustic emission signal. The change of the shape of the MAE signal envelope is very significant but the overall signal intensity is not strongly modified. Being so one has to look for some shape dependent parameters and two best candidates are the peak height ratio and pulse count ratio. Relative change of both of them is much higher than the sum of standard deviations obtained for the as-received and exploited samples.

References

[1] Mitra, A, Chen ZJ, Laabs F, Jiles DC. Micromagnetic Barkhausen emissions in 2·25 wt% Cr–1 wt% Mo steel subjected to creep. Philos Mag A 1997;75(3):847. https://doi.org/10.1080/01418619708207206

[2] Moorthy V, Shaw BA, Hopkins P. Magnetic Barkhausen emission technique for detecting the overstressing during bending fatigue in case-carburised En36 steel. NDT&E Int 2005;38:159. https://doi.org/10.1016/j.ndteint.2004.07.006

[3] Lord AE. Physical Acoustics 11:290. Ed. Mason WP, Thurston R.N, New York: Academic Press 1975

[4] Lo CCH, Scruby CB, Smith GDW. Dependences of magnetic Barkhausen emission and magnetoacoustic emission on the microstructure of pearlitic steel. Philos Mag 2004;84(18):1821. https://doi.org/10.1080/14786430410001663196
[5] Ng DHL, Jakubovics JP, Scruby CB, Briggs GAD. Effect of stress on magneto-acoustic emission from mild steel and nickel. J Magn Magn Mater 1992;104-107:355. https://doi.org/10.1016/0304-8853(92)90831-8
[6] Tochilin SB, Jakubovics JP, Briggs GAD. Use of magnetoacoustic emission for studying stress in industrial components. IEEE Trans Magn 1995;31(6):4163. https://doi.org/10.1109/20.489894
[7] Kostin VN, Vasilenko ON, Filatenkov DY, Chekasina YA, Serbin ED. Magnetic and magnetoacoustic testing parameters of the stressed–strained state of carbon steels that were subjected to a cold plastic deformation and annealing. Russ J Nondestruct Test 2015;51(10):624. https://doi.org/10.1134/S1061830915100071
[8] Su F. Methodology for the Stress Measurement of Ferromagnetic Materials by Using Magneto Acoustic Emission. Experimental Mechanics 2014;54(8):1431. https://doi.org/10.1007/s11340-014-9920-0
[9] Park. DG, Ok CI, Jeong HT, Kuk IH, Hong JH. Nondestructive evaluation of irradiation effects in RPV steel using Barkhausen noise and magnetoacoustic emission signals. J Magn Magn Mater 1999;196:382. https://doi.org/10.1016/S0304-8853(98)00766-5
[10] Augustyniak B, Piotrowski L, Chmielewski M, Sablik MJ. Microscopic impact of creep damage incipience and development on the magnetic properties of ferromagnetic Cr–Mo steel. J Magn Magn Mater 2006;304:e555. https://doi.org/10.1016/j.jmmm.2006.02.274
[11] Aghajani A, Somsen Ch, Pesicka J, Bendick W, Hahn B, Eggeler G. Microstructural evolution in T24, a modified 2(1/4)Cr–1Mo steel during creep after different heat treatments Mat Sci Eng A-Struct 2009;510–511:130. https://doi.org/10.1016/j.msea.2008.08.049
[12] Zieliński A,Golański G, Sroka M. Influence of long-term ageing on the microstructure and mechanical properties of T24 steel. Mat Sci Eng A-Struct 2017;682:664. https://doi.org/10.1016/j.msea.2016.11.087
[13] Augustyniak B, Piotrowski L, Chmielewski M, Kosmas K, Hristoforou E. Barkhausen Noise Properties Measured by Different Methods for Deformed Armco Samples. IEEE Trans Magn 2010;46(2):544. https://doi.org/10.1109/TMAG.2009.2033340
[14] Augustyniak B, Chmielewski M, Piotrowski L, Sablik MJ. Designing a magnetoacoustic emission measurement configuration for measurement of creep damage in power plant boiler tubes. J Appl Phys 2002;91(10):8897. https://doi.org/10.1063/1.1450851
[15] Augustyniak B, Chmielewski M, Piotrowski L, Sablik MJ. Nondestructive characterization of 2Cr-1Mo steel quality using magnetoacoustic emission. IEEE Trans Magn 2002;38(5):3207. https://doi.org/10.1109/TMAG.2002.802416

[16] Stupakov A, Farda R, Neslušan M, Perevertov A, Uchimoto T. Evaluation of a Nitrided Case Depth by the Magnetic Barkhausen Noise. J Nondestruct Eval 2017;36:73. https://doi.org/10.1007/s10921-017-0452-2
[17] Walnut DF. An Introduction to Wavelet Analysis, Boston, MA: Birkhäuser 2004